Cellulose (2019) 26:4853–4864
https://doi.org/10.1007/s10570-019-02411-2

ORIGINAL RESEARCH

Structural and functional modification of cellulose nanofibrils using graft copolymerization with glycidyl methacrylate by Fe^{2+}–thiourea dioxide–H_2O_2 redox system

Lifang Guo · Dongfang Li · Helena Lennholm · Huamin Zhai · Monica Ek

Received: 21 November 2018 / Accepted: 26 February 2019 / Published online: 16 April 2019

Abstract To graft epoxy and ester functional groups onto cellulose nanofibrils (CNFs) and to overcome their poor hydrophobicity, we studied the modification of CNFs using graft copolymerization with glycidyl methacrylate (GMA) by a Fe^{2+}–thiourea dioxide–H_2O_2 initiator system (Fe^{2+}–TD–H_2O_2) in aqueous solution. The synthesized poly (GMA)-grafted CNF (CNF-g-PGMA) was characterized by FTIR, AFM, XRD, water contact angle, and TGA. GMA was successfully grafted onto the CNFs by Fe^{2+}–TD–H_2O_2, the epoxy groups and ester groups of GMA were clearly present and intact in the CNF-g-PGMA, and TD is an important component of the initiator system under relatively mild graft conditions. CNF-g-PGMA may be an important intermediate because of its epoxy and ester functional groups. The main nanostructure of the CNFs was retained after graft copolymerization, and there were no obvious effects of graft copolymerization on the crystalline structure of the CNF backbone, although the crystalline index slightly decreased with the increased percentage of grafting. Graft copolymerization significantly modifies the CNF hydrophobicity. This strategy could extend the applications of CNFs into many areas.

L. Guo · H. Zhai (✉)
Jiangsu Provincial Key Lab of Pulp and Paper Science and Technology, Nanjing Forestry University, Nanjing, China
e-mail: hzhai@njfu.edu.cn

L. Guo · D. Li · H. Lennholm · M. Ek (✉)
Department of Fibre and Polymer Technology, School of Engineering Sciences in Chemistry, Bio Technology and Health, KTH Royal Institute of Technology, Stockholm, Sweden
e-mail: monicaek@kth.se

Graphical abstract

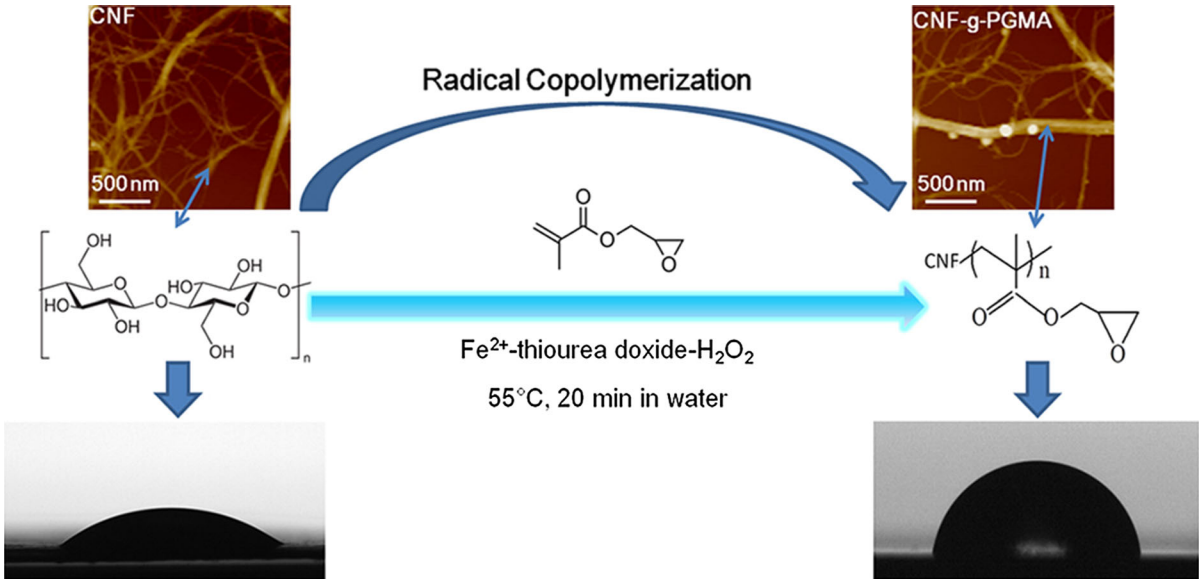

Keywords Cellulose nanofibrils · Modification · Glycidyl methacrylate · Graft copolymerization · Fe^{2+}–thiourea dioxide–H_2O_2

Introduction

Cellulose nanofibrils (CNFs), also known as nanofibrillated cellulose or microfibrillated cellulose, can be isolated from natural resources (such as wood, cotton, algae, and tunicate), and have widths ranging from 3 to 10 of nanometers and lengths on the micron scale, depending on the raw material and the preparation method (Habibi 2014). Because of their unique characteristics of high surface area, low density, mechanical and colloidal properties, and its renewable and biodegradable characteristics, CNFs have been widely used in applications such as paper, packaging, food, pharmaceutical and biomedical products, and energy storage (Jorfi and Foster 2015; Kargarzadeh et al. 2017). However, the abundant hydroxyl groups on the surface of CNFs make them a highly hydrophilic material, which can impair its excellent properties, as well as lead to some challenges, such as dispersion in non-polar matrices (Isogai 2015; Kargarzadeh et al. 2017; Klemm et al. 2011). Many polymer matrices are hydrophobic, and thus, it has been difficult to obtain uniformly nano-dispersed distributions of CNF in a hydrophobic matrix, resulting in very low or no improvement in compatibility and/or reinforcement of composite materials (Isogai 2015; Khalil et al. 2012; Yano et al. 2018). Therefore, efficient conversion from hydrophilic to hydrophobic properties is highly desirable in many cases to improve the dispersibility of CNFs.

Several previous approaches intended to improve interfacial interactions have been shown to obtain nanocellulose derivatives that disperse well in non-polar solvents and polymer matrices. Surface modification based on polymer grafting, coupling agents, acetylation, alkylation, and cationic modification have proved to be good methods to modify CNFs and tune their chemistry (Geng et al. 2018; Kargarzadeh et al. 2018; Navarro and Edlund 2017). Among the modification methods, graft copolymerization is an attractive and versatile method for the modification of polymer surfaces by imparting a variety of functional groups to a polymer (Roy et al. 2009). According to initiation mechanisms, cellulose graft copolymerization can be carried out using three approaches: attaching preformed polymer chains to the cellulose backbone (grafting onto), growing new polymer chains from radical sites on the backbone (grafting from), and introducing vinylic groups to cellulose and copolymerizing the resulting macro monomer with a

small molecular weight co-monomer (grafting through)(Odian 1981). Acrylic and vinyl graft copolymerization to cellulose backbone via a free radical mechanism generally involves the grafting-from approach.

Free radical copolymerization is a common polymerization method because of its many attractive characteristics, such as simple implementation, efficiency, and wide adaptability (Roy et al. 2009). The type of initiator exerts a remarkable effect on the grafting and it determines the grafting percentage, which sequentially influences the structure and properties of the products. In the grafting of vinyl monomers onto cellulose or cellulose derivatives, the initiation can be performed by chemical initiators or by irradiation/radiation. Chemical initiators (Missoum et al. 2013; Wei and Mcdonald 2016), redox initiators such as ceric ammonium nitrate (CAN) (Littunen et al. 2011; Spinella et al. 2016), Fenton's reagent (Fe^{2+}–H_2O_2) (Ibrahim et al. 2010), and free radical generators such as various persulfates and azobisisobutyronitrile are most commonly used. Redox initiator systems can be used at low temperatures and in aqueous media, and they react only with the amorphous region of cellulose because it is more reactive than the crystalline phase of cellulose. Fe^{2+}–H_2O_2 is highly reactive, non-selective, cheap, and easily available (Kalia and Sabaa 2013). It has been used for grafting vinyl monomers onto cellulose, starch, gelatin, and natural rubber (Kalia and Sabaa 2013). Thiourea dioxide (TD) has been utilized as an effective reducing agent in the textile printing, paper, photographic, and leather processing industries for a long time. It has also been used in academic research towards organocatalytic, polymerization, and phase-transfer reactions, and for the reduction of graphene and graphite oxides (Makarov et al. 2015). The reduction process generates sodium sulfite and urea, which are easy to manage because these are common commercial wastes. Moreover, TD is easily available in bulk quantities, and is safer and less expensive than other reducing agents. TD-assisted Fenton's reagent has been proved to modify macro fibers more efficiently than Fenton's reagent (Waly et al. 1982). Although Fe^{2+}–H_2O_2 with or without a third component assist has been used as an initiator to modify macro fibers (El-Alfy et al. 1985; Misra et al. 1979) and cellulose nanocrystals (Spinella et al. 2016), there are few reports of its being used with CNFs.

Glycidyl methacrylate (GMA) is an attractive monomer because of its bifunctional groups: a double bond that is reactive with free radicals together with an epoxy group that can react with a number of other functional groups, such as carboxyl, hydroxyl, anhydride, and amine. Therefore, functionalization via grafting GMA with polymers such as polypropylene (Wang et al. 2018), polyethylene (Li et al. 2018), polystyrene (Wang et al. 2018), polylactide (Kumar et al. 2010) and graphene oxide (Osicka et al. 2018) has attracted wide attention. Up to now, there are few reports of structural and functional modification of cellulose nanofibrils using graft copolymerization of CNFs with GMA by a Fe^{2+}–TD–H_2O_2 redox system.

We studied graft copolymerization of CNFs with GMA induced by TD-assisted Fe^{2+}–H_2O_2 (Fe^{2+}–TD-H_2O_2). A poly(GMA)-functionalized CNF derivatives (CNF-g-PGMA) with epoxy group and ester bond structure was synthesized in an environmentally friendly aqueous process. The chemical structure, morphology, crystalline structure, hydrophobicity and thermal stability of the products were studied in detail. The products became less hydrophilic after grafting. Their chemistry and application are extended because of the addition of active epoxy groups and ester bonds.

Experimental

Materials

CNF suspensions (~ 10 wt%) were commercial source, supplied by a Norway company. The sample was diluted to 1.0 wt% by deionized water and then fully mechanically disintegrated by a microfluidizer (M-110EH, Microfluidics Crop, United States) with smaller chambers (200 μm and 100 μm) at 1600 bar for three passes. The resulted CNFs have an average width of 21 nm and lengths of serval micrometers. Glycidyl methacrylate (GMA) was stored at 4 °C and filtered through aluminum oxide to remove inhibitor before use. Thiourea dioxide (TD), ferrous ammonium sulfate (FAS, $FeSO_4$ $(NH_4)_2SO_4{\cdot}6H_2O$), hydrogen peroxide (H_2O_2, 30 wt%) and acetone were used as received. All the chemicals were obtained from Sigma-Aldrich. Deionized water was used in all processes.

Graft copolymerization

The method for GMA graft copolymerization on CNFs initiated by Fe^{2+}–H_2O_2–TD was performed following a procedure described elsewhere (Huang and Zhai 2008), with slight changes. A suspension of CNFs in water (1.0 wt%, 100 g), FAS (0.012 g), TD (0.25 g), and GMA (2–40 mmol/g CNFs) was added to a 250-mL flask and stirred for 15 min under nitrogen atmosphere. Then, H_2O_2 (50 μL) was added and the mixture was heated to 55 °C while stirring. After reaching 55 °C, the reaction was allowed to continue for 20 min under nitrogen atmosphere. CNFs treated only with the initiators was used as a control sample (CNF-control).

Removal of homopolymers

Immediately after the graft copolymerization reaction, the mixture, including copolymers (poly-GMA-grafted CNFs, CNF-g-PGMA), homopolymers (poly-glycidyl methacrylate, PGMA), unreacted monomers (GMA), and initiators was washed with deionized water and three successive centrifugation steps at 4000 rpm for 5 min to remove the initiators and monomers. The copolymers and homopolymers were separated by Soxhlet extraction with acetone (O'Connell et al. 2010) for 24 h. After the extraction, the copolymers were washed with deionized water and three successive centrifugation steps at 4000 rpm for 5 min to exchange acetone with deionized water. Then, the aqueous suspensions of copolymers were diluted to 0.5 wt% and homogenized using a T18 Digital Ultra Turrax Basic Homogenizer (IKA, United States) at 12,000 rpm for 10 min for further use. The homopolymers in acetone were collected for characterization as well.

Characterization

Gravimetric calculations

The grafting percentage (G), grafting efficiency (E), and monomer conversion (C) were calculated using the following equations:

$$G(\%) = \frac{m_2 - m_0}{m_0} \times 100 \quad (1)$$

$$E(\%) = \frac{m_2 - m_0}{m_1 - m_0} \times 100 \quad (2)$$

$$C(\%) = \frac{m_1 - m_0}{m_m} \times 100 \quad (3)$$

where m_0 *is* the mass of initial CNFs; m_1 is the mass of total polymers, including homopolymers and copolymers; m_2 is the mass of copolymers after removing homopolymers by Soxhlet extraction and m_m is the initial mass of GMA monomer.

Fourier transform infrared spectroscopy (FTIR)

FTIR was carried out on the starting material and all modified products using a Fourier transform infrared spectroscopy spectrometer (PerkinElmer Spectrum 2000, Waltham, MA, United States) equipped with an attenuated total reflectance (ATR) system. The spectra were recorded using the spectral range 600–4000 cm^{-1} with 4 cm^{-1} resolution over 16 scans. All the spectra were obtained from dry film samples at room temperature.

Atomic force microscopy (AFM)

AFM samples were prepared from very dilute dispersions by putting a drop on a clean silicon slice surface and drying at room temperature. The morphology of unmodified and modified CNFs was analyzed by AFM (Multimode8, Veeco, Santa Barbara, CA, United States) with ScanAsyst in air mode. Silicon cantilevers (Veeco) with a radius of 8 nm were used. The drive frequency was between 200 and 400 kHz. The width of CNFs was assessed by analyzing the AFM height image using NanoScope Analysis software, in which the heights of around 200 nanofibrils were measured.

Field emission scanning electron microscopy (FE-SEM)

FE-SEM (S-4800, Hitachi, Japan) was used to image unmodified and modified CNF samples. The samples were prepared from unmodified and modified CNF suspensions (in water or in acetone). The samples were drop-coated on a clean silicon slice and dried in air. Before imaging, all samples were coated with 3 nm of Pt/Pd using a Cressington 208HR high-resolution sputter coater. FE-SEM was performed using an

acceleration voltage of 1 kV and an electric current of 10 μA.

X-ray diffraction (XRD)

XRD was used to determine the crystallinity of different samples. Each sample was freeze-dried and milled into fine powder before the determination. Each sample in the form of milled powder was placed on the sample holder and leveled to obtain total and uniform X-ray exposure. XRD patterns were recorded by monitoring the diffraction angle 2θ from 5° to 40° on an X-ray diffraction meter equipped with an X'Celerator detector (PANalytical X'Pert PRO, Panalytical, Netherlands) using CuKα radiation (k = 0.154 nm) at 45 kV and 45 mA. The slit system was 1° for divergence, 0.15 mm for receiving and 1° for scatter. The scanning speed was 5°/min. The crystalline index (CI) was calculated from the ratio of the intensity of the 200 peak (I_{200}, 2θ = 22.6°) and the intensity of the minimum (I_{AM}, 2θ = 18°) between the 200 and 110 peaks, as shown in Eq. 4 (Segal et al. 1959). I_{200} represents both crystalline and amorphous material, whereas I_{AM} represents the amorphous material.

$$\mathrm{CI} = \frac{I_{200} - I_{AM}}{I_{200}} \times 100\% \quad (4)$$

Water contact angle

The hydrophobicity of unmodified and modified samples was characterized by static water contact angle. Each of the 0.5 wt% suspension samples prepared above was casted on Petri dishes and dried at room temperature to make cast films. The Petri dishes were placed on a level surface before drying to ensure a uniform thickness of films. The water contact angle was measured with a 5 μL deionized water droplet at ambient temperature by using a contact angle meter (CAM200, KSV Instruments LTD, Sweden). The values of contact angle were obtained as averages of at least five liquid drops on different points of the sample.

Thermal gravimetric analysis (TGA)

The thermal stability of the various samples was determined by a TGA instrument (SDTA 851e, Mettler Toledo, Swiss). Freeze-dried samples weighing between 5.0 and 6.0 mg were placed in 100 μL alumina crucibles and heated at a heating rate of 10 °C/min and a heating range from 30 to 600 °C under a dynamic N_2 flow rate of 50 mL/min. Each sample was tested in duplicate.

Results and discussion

CNF-g-PGMA structure

Factors that can affect grafting include the nature of the backbone, the pretreatment of cellulose substrate with initiator or a swelling agent, the type of solvent or grafting medium (homogeneous or heterogeneous), the monomer level, the dosage of initiators, temperature, the grafting duration, the presence or absence of oxygen during grafting, and the stirring speed, when the raw materials, monomer, and initiators are fixed. In the present study, only the monomer level was considered, while the other conditions were fixed throughout the experiments. The grafting percentage and the morphology are dependent on the amount of monomer. It can be seen from the FTIR spectrum that the grafting percentage increases with an increase in the monomer level, as the absorption intensity increases greatly. When the monomer dosage was 20 mmol/g, the grafting percentage was 72% by gravimetric calculation, the grafting efficiency was 28% and the monomer conversion was 91%. The grafting efficiency was not as high as in some other reports in the literature. This is probably because of free Fe^{2+} in the solution; when the same initiator was used to treat macro fibers, Fe^{2+} was absorbed on the cellulose substrate. Fe^{2+} was added directly into the CNF suspension instead of using Fe^{2+} to pretreat the CNF, as it is not easy to separate free Fe^{2+} and adsorbed Fe^{2+}. Theoretically, a higher grafting percentage can be obtained by adjusting the factors.

TD did promote the grafting, as experiments were carried out without TD under the same reaction conditions with a monomer amount of 30 mmol/g and almost no grafting occurred. During the experimental process, GMA liquid could still be observed at the end of the reaction and no relative absorption peaks could be observed on the FTIR spectrum. The Fe^{2+}–H_2O_2 system failed to initiate graft copolymerization under the same condition, which indicated that reaction (7) prevailed over reaction (5). Thus, reaction

(6) was inhibited. The graft copolymerization was successfully initiated in the Fe^{2+}–H_2O_2–TD system, which was probably due to the reaction of TD with H_2O_2, and the reaction of $HO^{\cdot}$ free radical and Fe^{3+} with TD produced other free radicals, namely reaction (8) ∼ (10). In addition, TD also reduced Fe^{3+} to Fe^{2+}, which facilitated the reaction (5). The free radical $HN{=}C(NH_2){-}SO_2^{\cdot}$ reacted with cellulose to generate cellulose macromolecular radicals and TD, as shown in reaction (11). The cellulose macromolecular radicals generated by the reaction (6) ∼ (11) were captured by GMA monomer, which led to the graft copolymerization.

$$H_2O_2 + Fe^{2+} \rightarrow HO^- + HO^{\bullet} + Fe^{3+} \quad (5)$$

$$HO^{\bullet} + Cell - OH \rightarrow H_2O^- + Cell - O^{\bullet} \quad (6)$$

$$HO^{\bullet} + Fe^{2+} \rightarrow HO^- + Fe^{3+} \quad (7)$$

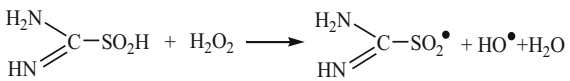

(8)

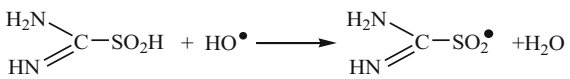

(9)

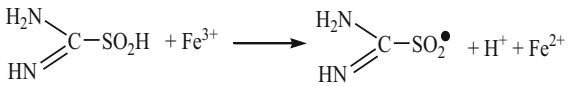

(10)

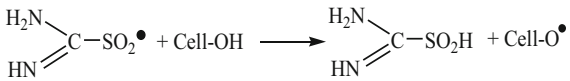

(11)

The chemical structures of initial CNFs, modified CNFs, and neat PGMA were characterized by FTIR, as displayed in Fig. 1. It can be observed that GMA was successfully grafted on the CNFs. The peaks at 3334 (hydrogen bond bending), 2910 (C–H stretching), 1648-1620 (OH bending from absorbed water), 1435 (C–H deformation), 1160 (C–O–C stretching), 1375-1030 (C–O stretching), and 895 (stretch C_1–O–C_4) cm^{-1}, which are typical bands of native cellulose,

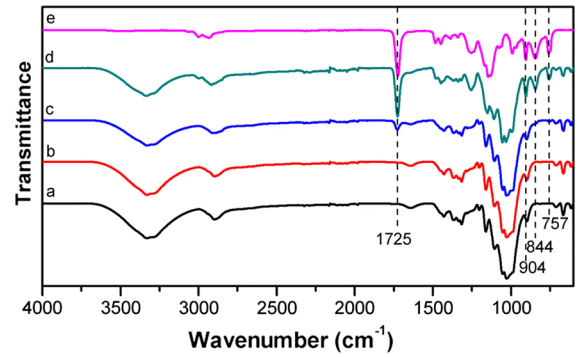

Fig. 1 FTIR spectra of (a) initial CNFs, (b) CNF-control (reacting without monomers), (c) CNF-g-PGMA with a monomer level of 7 mmol/g, (d) CNF-g-PGMA with a monomer level of 30 mmol/g and (e) neat PGMA

were observed for the initial CNFs. In the spectrum of CNF-control (Fig. 1b), which was only reacted with the initiators, there is no change compared to the initial CNFs. This shows that the chemical structure of CNFs is not affected by the treatment with initiators. For PGMA, the absorption peak at 1723 cm^{-1} in the spectrum Fig. 1e is ascribed to the C=O stretching vibration (Mao and Gleason 2004). The epoxy groups can be identified by the absorption peaks at 905, 844, and 758 cm^{-1}(Griffiths 1991). The absence of a peak at around 1640 cm^{-1}, which can be assigned to C=C stretching vibration, shows that there was no monomer left in the homopolymers. Compared with unmodified CNFs, there are several new absorption bands for the modified CNF samples. The characteristic peak at 1725 cm^{-1} is assigned to C=O stretching vibration, indicating the presence of ester groups of GMA. The peaks at 904, 844, and 757 cm^{-1} show that epoxy groups were introduced on the CNFs and are intact. The intensity increases greatly with an increase in the monomer level.

Morphology

Figure 2 shows the AFM height images of native CNFs and modified CNFs. The width of the initial CNFs ranges from 3 to 50 nm, with an average of 21 nm and the length is several micrometers. Compared with the unmodified CNFs, the nanoscale structure of fibrils is maintained after graft copolymerization. Many small particles can be observed on the surface of grafted CNFs with diameters ranging from 20 to 200 nm. No obvious relationship between

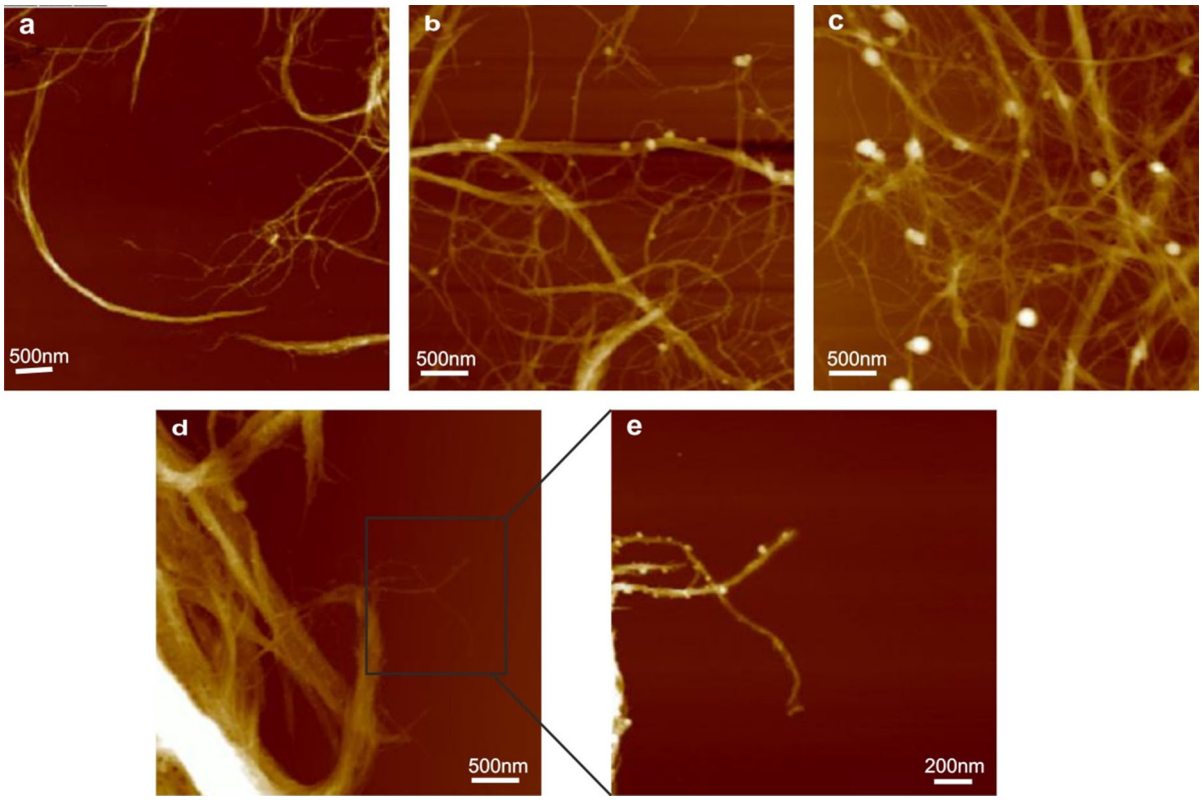

Fig. 2 AFM height images of **a** initial CNFs, **b** CNF-g-PGMA with a monomer amount of 7 mmol/g, **c** CNF-g-PGMA with a monomer amount of 10 mmol/g, and **d, e** CNF-g-PGMA with a monomer amount of 30 mmol/g

the diameter of particles and the grafting percent is observed, whereas the number of particles increases with increasing grafting percent. However, as shown in Fig. 2d, the fibrils seem to be adhered together with the polymers. The fibrils probably crosslinked and aggregated by radical polymerization by side chains grafted on CNFs, according to the chain transfer mechanism.(Roy et al. 2009). When the monomer level is relatively low, no aggregation occurs; the aggregation at high monomer level would probably be preventable by adding the GMA gradually. In addition, it seems the modification happened periodically along the axis of CNF, especially shown in Fig. 2e, primarily at the amorphous regions (Battista 1950). That indicates that the amorphous regions are more accessible to the reagents used in the reaction. This is consistent with previous studies (Henriksson et al. 2005).

SEM images of initial CNFs and modified CNFs dispersed in water or acetone are shown in Fig. 3. When CNFs are dispersed in the less polar solvent acetone, the fibrils seem more independent from each other than those in water. When CNF-g-PGMA is dispersed in acetone, which is a good solvent for PGMA, the grafted PGMA on the fibrils is dissolved and forms a membrane after drying, as shown in Fig. 3c. No pores like those in Fig. 3b are observed. This indicates that it is probably feasible to use solvents which are less polar than water to disperse CNFs after copolymerization.

Crystal structure

XRD patterns of unmodified CNFs, modified CNFs, and PGMA are shown in Fig. 4. For native CNFs, the typical cellulose I crystal structure is displayed, with broad peaks centered at 16° corresponding to (1–10) and (110) planes, a sharp peak at 22.4° corresponding to the (200) plane and a peak at 34.5° corresponding to the (004) plane (French 2014; Okita et al. 2010). The crystallinity index of the initial CNFs was 63.2%. For the CNF-control sample, treated only by the initiators,

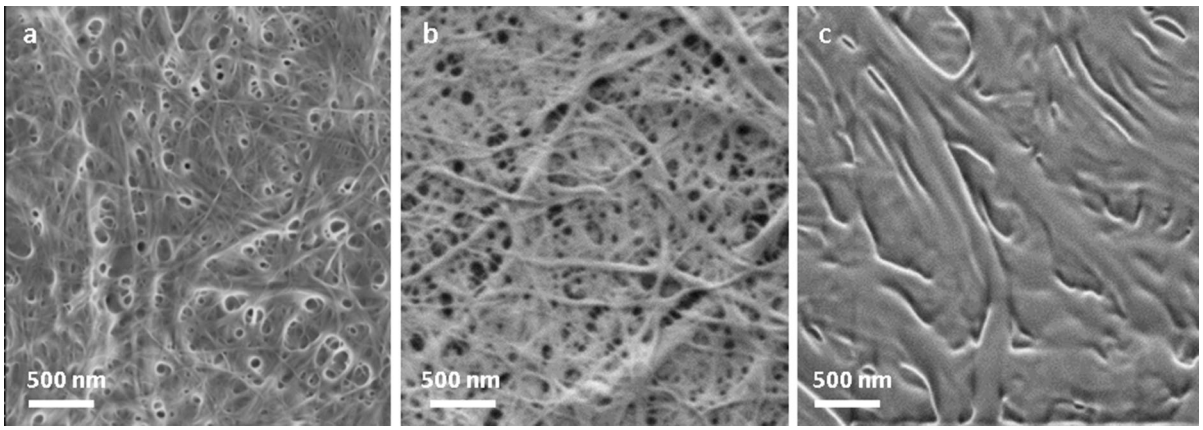

Fig. 3 SEM images of **a** initial CNFs dispersed in water, **b** initial CNFs dispersed in acetone, and **c** CNF-g-PGMA with a monomer amount of 30 mmol/g dispersed in acetone

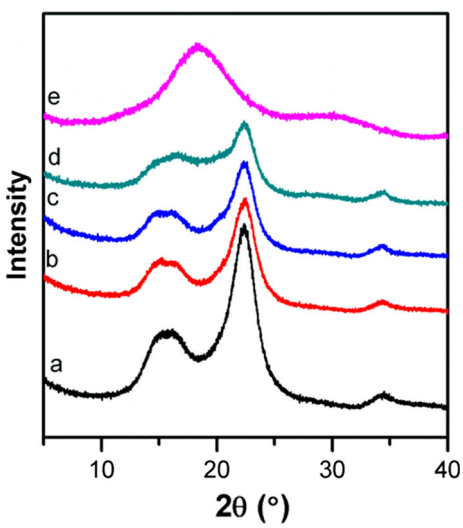

Fig. 4 XRD patterns of (a) initial CNFs, (b) CNF-control, (c) CNF-g-PGMA with a monomer amount of 7 mmol/g, (d) CNF-g-PGMA with a monomer amount of 30 mmol/g, (e) PGMA

the crystal structure did not change, while the crystallinity index slightly decreased to 62.5%. This reduction suggests that the initiator reagents were able to slightly damage the crystalline structure, which probably produced more active sites for grafting. Compared with other initiators, such as ceric initiator (Bo et al. 2015), there was no more damage of the crystalline structure. For PGMA, there is an amorphous diffraction peak centered at around 18.3°. Compared with unmodified CNFs, CNF-g-PGMA shows similar patterns, and the crystallinity index slightly decreases to 59.9%. This indicates that the original crystal structure was preserved after grafting with PGMA and the graft copolymerization occurred mainly on the surfaces of CNFs. For modified CNFs with a higher monomer amount of 30 mmol/g, as shown in Fig. 4d, the cellulose peaks overlap with the amorphous diffraction peak of PGMA, and the crystallinity index is estimated to be 36.3%. This indicates that the crystallinity index of modified CNFs decreases with increasing grafting percentage of amorphous PGMA.

Hydrophobicity

The water contact angle results are given in Fig. 5. The static contact angle shows that graft copolymerization significantly changes the surface wetting characteristics of CNFs. The initial CNFs film presents a relatively low contact angle value of 31°, due to its hydrophilic surface. The CNF-g-PGMA becomes more hydrophobic with increasing monomer amount. A maximum contact angle of 81° was obtained for the film consisting of CNF-g-PGMA with a monomer amount of 40 mmol, which was a bit higher than that of neat PGMA film with a contact angle value of 77°. During the preparation process, it was observed that dewatering became much easier for modified CNFs by filtration or centrifuging, even at a very low grafting percentage (i.e. the monomer amount of 2.0 mmol/g). The improved dewatering ability of modified CNFs could be of benefit for some subsequent applications, such as water treatment.

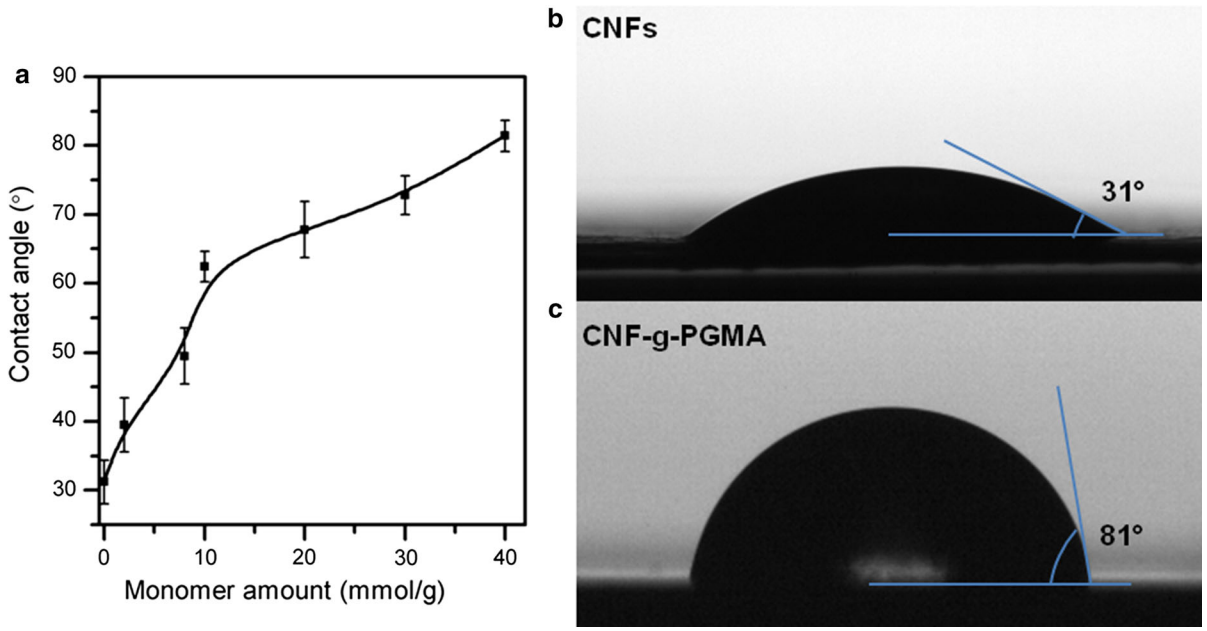

Fig. 5 Effect of grafting copolymerization on contact angle

Thermal stability

The thermal decomposition behavior of neat CNFs, modified CNFs and neat PGMA was characterized by TGA. Figure 6 gives TGA curves and the corresponding derivative thermogravimetric (DTG) curves. As shown in Fig. 6a, b, the thermal degradation of initial CNFs proceeded rapidly at 230–400 °C, with the degradation peak temperature at 350 °C. The onset degradation temperature (T_{onset}, values determined at 5% weight loss on the TGA curves) of CNFs was 295 °C, and the char residual yield of unmodified CNFs at 600 °C was about 17 wt%. For the CNF-control sample, which was only treated by the initiators, T_{onset} remained at 295 °C. It was previously shown that cellulose nanocrystals (CNCs) oxidized with ceric initiator exhibit a lower onset temperature (shift from 295 °C for unmodified CNCs to 250 °C for the ceric oxidized CNCs)(Kedzior et al. 2016). Compared with ceric oxidized samples, the initiator showed less effect on the onset temperature. However, the degradation peak temperature decreased to 335 °C and the char residual yield decreased to 13 wt%. This can probably be attributed to the decrease in crystallinity (Poletto et al. 2012). The thermal decomposition of neat PGMA proceeded in three separate pyrolysis processes: a primary decomposition process at 140–220 °C followed by a main process at 220–360 °C and a final slow charring process at 360–480 °C. For modified CNFs, the T_{onset} shifted from 295 to 275 °C, because of the low T_{onset} of PGMA. As the grafting percentage increased, the T_{onset} remained at around 275 °C. The temperature of maximum decomposition rate in CNF-g-$PGMA_7$ was 334 °C, which is the same as that of the CNF-control. For CNF-g-$PGMA_{30}$, three degradation peaks (180, 320, and 358 °C respectively) were observed, as shown in Fig. 6d. In conclusion, polymer grafted CNFs exhibited decreased thermal stability compared to unmodified CNFs. The modification broadened the melt process window, as the degradation peak temperature showed characteristics of both CNFs and PGMA.

Conclusions

GMA was successfully grafted onto CNFs by using a Fe^{2+}–TD–H_2O_2 initiator system and TD is an important component of the initiator system under the relative mild graft conditions. The main nanostructure of the CNFs in CNF-g-PGMA was retained after the graft copolymerization. The graft copolymerization has little effect on the crystalline structure of the CNF

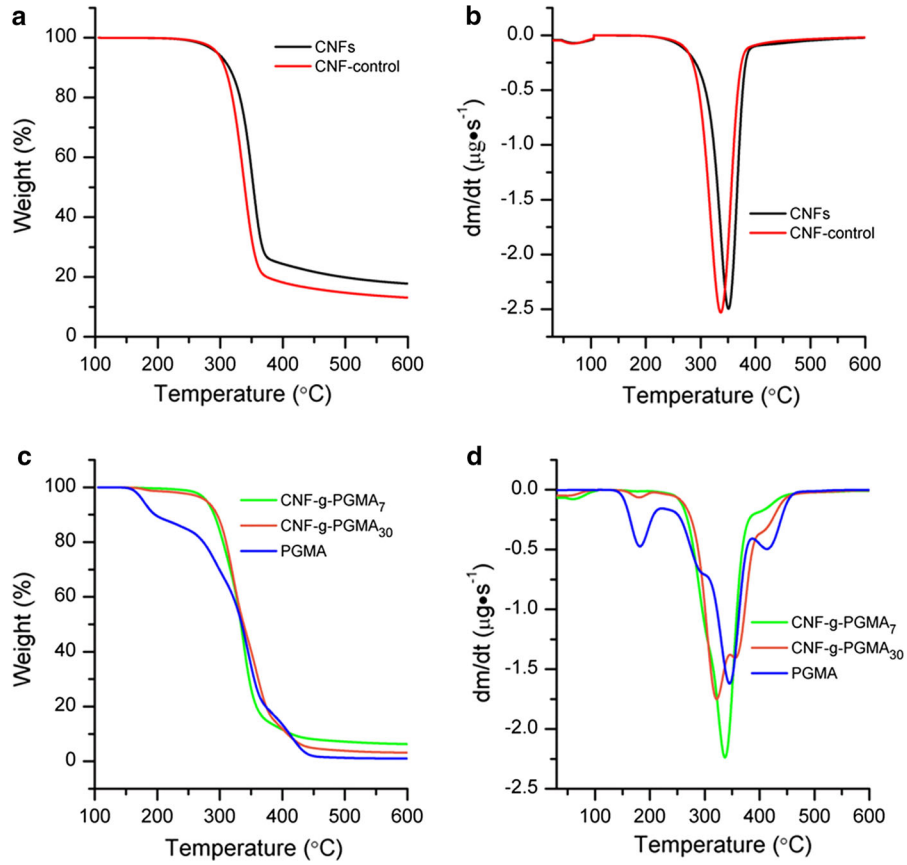

Fig. 6 TGA and DTG curves of unmodified CNFs, modified CNFs (CNF-g-$PGMA_7$ is the sample with a monomer amount of 7 mmol/g, CNF-g-$PGMA_{30}$ the sample with a monomer amount of 30 mmol/g), and PGMA

backbone in CNF-g-PGMA. CNF-g-PGMA may be an important intermediate due to its attached epoxy and ester functional groups. The graft copolymerization significantly modifies the CNF hydrophobicity. This may extend the functional applications of CNFs in many fields, and further research on developing applications is under way.

Acknowledgments The authors are grateful for the support of the National Natural Science Foundation of China (Grant No. 31070524), and the Major State Basic Research Development Program of China (Grant No. 2010CB732205).

References

Battista OA (1950) Hydrolysis and crystallization of cellulose. Ind Eng Chem 42:502–507. https://doi.org/10.1021/ie50483a029

Bo S, Hou Q, Liu Z, Ni Y (2015) Sodium periodate oxidation of cellulose nanocrystal and its application as a paper wet strength additive. Cellulose 22:1135–1146. https://doi.org/10.1007/s10570-015-0575-5

El-Alfy E, Waly A, Hebeish A (1985) Graft copolymerization of perfluoroheptyl methacrylate/glycidyl methacrylate mixtures with cotton fabric using Fe^{2+}-thioureadioxide-H_2O_2 redox system. Macromol Mater Eng 130:137–146. https://doi.org/10.1002/apmc.1985.051300111

French AD (2014) Idealized powder diffraction patterns for cellulose polymorphs. Cellulose 21:885–896. https://doi.org/10.1007/s10570-013-0030-4

Griffiths PR (1991) The handbook of infrared and Raman characteristic frequencies of organic molecules. Academic Press, New York. https://doi.org/10.1016/0924-2031(92)87021-7

Habibi Y (2014) Key advances in the chemical modification of nanocelluloses. Chem Soc Rev 43:1519–1542. https://doi.org/10.1039/c3cs60204d

Henriksson G, Christiernin M, Agnemo R (2005) Monocomponent endoglucanase treatment increases the reactivity of softwood sulphite dissolving pulp. J Ind Microbiol Biot 32:211–214. https://doi.org/10.1007/s10295-005-0220-7

Huang J, Zhai HM (2008) Graft copolymerization of glycidyl methacrylate with eucalyptus pulp induced by Fe^{2+}–H_2O_2–thiourea dioxide redox system. Chem Ind For Prod 28:58–62. http://www.cifp.ac.cn/EN/Y2008/V28/I2/58

Ibrahim NA, Wan MZWY, Abu-Ilaiwi FA, Rahman MZA, Ahmad MB, Dahlan KZM (2010) Graft copolymerization of methyl methacrylate onto oil palm empty fruit bunch

fiber using H_2O_2/Fe^{2+} as an initiator. J Appl Polym Sci 89:2233–2238. https://doi.org/10.1002/app.12467
Isogai A (2015) Structural characterization and modifications of surface-oxidized cellulose nanofiber. J Jpn Pet Inst 58:365–375. https://doi.org/10.1627/jpi.58.365
Jorfi M, Foster EJ (2015) Recent advances in nanocellulose for biomedical applications. J Appl Polym Sci 132:41719. https://doi.org/10.1002/app.41719
Kalia S, Sabaa MW (2013) Polysaccharide based graft copolymers. Springer, Berlin. https://doi.org/10.1007/978-3-642-36566-9
Kargarzadeh H, Mariano M, Huang J, Lin N, Ahmad I, Dufresne A, Thomas S (2017) Recent developments on nanocellulose reinforced polymer nanocomposites: a review. Polymer 132:368–393. https://doi.org/10.1016/j.polymer.2017.09.043
Kargarzadeh H et al (2018) Advances in cellulose nanomaterials. Cellulose 25:1–39. https://doi.org/10.1007/s10570-018-1723-5
Kedzior SA, Graham L, Moorlag C, Dooley BM, Cranston ED (2016) Poly(methyl methacrylate)-grafted cellulose nanocrystals: one-step synthesis, nanocomposite preparation, and characterization. Can J Chem Eng 94:811–822. https://doi.org/10.1002/cjce.22456
Khalil HPSA, Bhat AH, Yusra AFI (2012) Green composites from sustainable cellulose nanofibrils: a review. Carbohydr Polym 87:963–979. https://doi.org/10.1016/j.carbpol.2011.08.078
Klemm D, Kramer F, Moritz S, Lindstrom T, Ankerfors M, Gray D, Dorris A (2011) Nanocelluloses: a new family of nature-based materials. Angew Chem Int Ed 50:5438–5466. https://doi.org/10.1002/anie.201001273
Kumar M, Mohanty S, Nayak SK, Rahail PM (2010) Effect of glycidyl methacrylate (GMA) on the thermal, mechanical and morphological property of biodegradable PLA/PBAT blend and its nanocomposites. Bioresour Technol 101:8406–8415. https://doi.org/10.1016/j.biortech.2010.05.075
Li X, Xu H, Long S, Yuan Y, Wang P, Qiu D, Ke K (2018) Improved compatibility in Recycled-PE/LDPE using glycidyl methacrylate, acrylic acid grafted mPE. Polym Test. https://doi.org/10.1016/j.polymertesting.2018.06.008
Littunen K, Hippi U, Johansson LS, Österberg M, Tammelin T, Laine J, Seppälä J (2011) Free radical graft copolymerization of nanofibrillated cellulose with acrylic monomers. Carbohydr Polym 84:1039–1047. https://doi.org/10.1016/j.carbpol.2010.12.064
Makarov SV, Horvath AK, Silaghi-Dumitrescu R, Gao Q (2015) Recent developments in the chemistry of thiourea oxides. Chem Eur J 46:14164–14176. https://doi.org/10.1002/chem.201403453
Mao Y, Gleason KK (2004) Hot filament chemical vapor deposition of poly(glycidyl methacrylate) thin films using tert-butyl peroxide as an initiator. Langmuir 20:2484–2488. https://doi.org/10.1021/la0359427
Misra BN, Dogra R, Kaur I, Jassal JK (1979) Grafting onto cellulose. IV. Effect of complexing agents on fenton's reagent (Fe^{2+}–H2O2)-initiated grafting of poly(vinyl acetate). J Polym Sci Polym Chem Ed 17:1861–1863. https://doi.org/10.1002/pol.1979.170170631
Missoum K, Belgacem MN, Bras J (2013) Nanofibrillated cellulose surface modification: a review. Materials 6:1745–1766. https://doi.org/10.3390/ma6051745
Navarro JRG, Edlund UM (2017) A surface-initiated controlled radical polymerization approach to enhance nanocomposite integration of cellulose nanofibrils. Biomacromolecules 18:1947–1955. https://doi.org/10.1021/acs.biomac.7b00398
O'Connell DW, Birkinshaw C, O'Dwyer TF (2010) A chelating cellulose adsorbent for the removal of Cu(II) from aqueous solutions. J Appl Polym Sci 99:2888–2897. https://doi.org/10.1002/app.22568
Odian GG (1981) Principles of polymerization. Wiley, NewYork
Okita Y, Saito T, Isogai A (2010) Entire surface oxidation of various cellulose microfibrils by TEMPO-mediated oxidation. Biomacromolecules 11:1696–1700. https://doi.org/10.1021/bm100214b
Osicka J, Mrlik M, Ilcikova M, Hanulikova B, Urbanek P, Sedlacik M, Mosnacek J (2018) Reversible actuation ability upon light stimulation of the smart systems with controllably grafted graphene oxide with poly (glycidyl methacrylate) and PDMS elastomer: effect of compatibility and graphene oxide reduction on the photo-actuation performance. Polym Basel 10:832. https://doi.org/10.3390/polym10080832
Poletto M, Zattera AJ, Forte MM, Santana RM (2012) Thermal decomposition of wood: influence of wood components and cellulose crystallite size. Bioresour Technol 109:148–153. https://doi.org/10.1016/j.biortech.2011.11.122
Roy D, Semsarilar M, Guthrie JT, Perrier S (2009) Cellulose modification by polymer grafting: a review. Chem Soc Rev 38:2046–2064. https://doi.org/10.1039/B808639G
Segal L, Creely JJ, Martin AE, Conrad CM (1959) An empirical method for estimating the degree of crystallinity of native cellulose using the X-ray diffractometer. Text Res J 29:786–794. https://doi.org/10.1177/004051755902901003
Geng S, Yao K, Zhou Q, Oksman K (2018) High-strength, high-toughness aligned polymer-based nanocomposite reinforced with ultra-low weight fraction of functionalized nanocellulose. Biomacromolecules 19:4075–4083. https://doi.org/10.1021/acs.biomac.8b01086
Spinella S, Samuel C, Raquez JM, Mccallum SA, Gross R, Dubois P (2016) Green and efficient synthesis of dispersible cellulose nanocrystals in biobased polyesters for engineering applications. ACS Sustain Chem Eng 4:2517–2527. https://doi.org/10.1021/acssuschemeng.5b01611
Waly A, Abou-Zeid NY, El-Alfy EA, Hebeish A (1982) Polymerization of glycidyl methacrylate, methacrylic acid, acrylamide and their mixtures with cotton fabric using fe^{2+}-thioureadioxide-H2O2redox system. Macromol Mater Eng 103:61–76. https://doi.org/10.1002/apmc.1982.051030106
Wang Y, Zhou J, Wu C, Tian L, Zhang B, Zhang Q (2018) Fabrication of micron-sized BSA-imprinted polymers with outstanding adsorption capacity based on poly(glycidyl methacrylate)/polystyrene (PGMA/PS) anisotropic

microspheres. J Mater Chem B 6:5860–5866. https://doi.org/10.1039/c8tb01423j

Wei L, Mcdonald AG (2016) A Review on grafting of biofibers for biocomposites. Materials 9:303. https://doi.org/10.3390/ma9040303

Yano H, Omura H, Honma Y, Okumura H, Sano H, Nakatsubo F (2018) Designing cellulose nanofiber surface for high density polyethylene reinforcement. Cellulose 25:3351–3362. https://doi.org/10.1007/s10570-018-1787-2